The interplay between cation ordering and elasticity of omphacites to unravel P-T-t paths of metamorphic rocks

Lisa Baratelli

Department of Earth Sciences "A. Desio", University of Milano, Via Botticelli 23, 20133, Milano

DOI: 10.19276/plinius.2025.01.001

INTRODUCTION

Clinopyroxenes (general formula $M1M2T_2O_6$) are widespread rock-forming minerals that occur in a variety of geological settings and processes. This makes them promising candidates for elastic geothermobarometry, a method that uses strain recorded by mineral inclusions to determine the pressure (*P*) and temperature (*T*) conditions of entrapment (Angel et al., 2019; Gilio et al., 2021). Among clinopyroxenes, omphacite inclusions are particularly valuable for constraining *P-T* conditions in eclogitic metabasites, where other inclusions such as quartz are absent as equilibrium phases at peak metamorphic conditions. Raman spectroscopy is one of the most used techniques to determine the pressures of inclusions for elastic geothermobarometry because it has the advantage of probing micrometer-scale regions without the need to extract the inclusion from the host. Raman scattering is highly sensitive to structural deformations, offering significant information about variations in the crystal structure caused by thermal or compressive stress. However, since omphacite is a solid solution, the positions of the Raman peaks are influenced by both the chemical composition and the degree of cation order, as well as *P*. This has so far prevented omphacites from being used for elastic geothermobarometry.

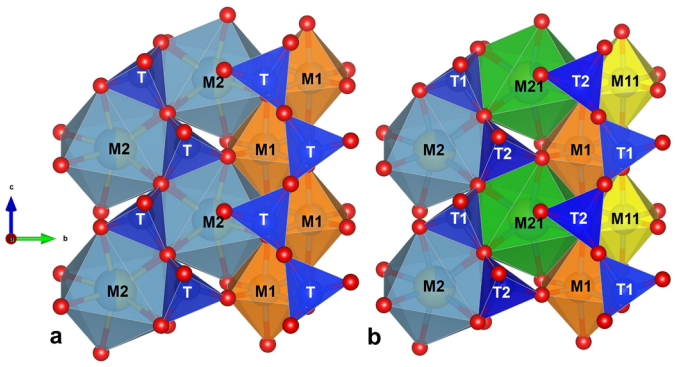

Figure 1 a) *Structural fragment of disordered (space group C2/c) and* ***b)*** *of disordered (P2/n) omphacite. SiO_4 tetrahedra are shown in dark blue, M1 sites in orange, M11 in yellow, M2 in light blue, and M21 in green. The diagrams (Baratelli et al., 2025a) were prepared using the VESTA software package (Momma & Izumi, 2008).*

The *P* and *T* conditions of the inclusion entrapment (P-T_{trap}) can be estimated knowing the inclusion *P* (P_{inc}), which affects the positions of the Raman peaks, and the elastic properties of both the host and the inclusion. These parameters define a line in *P-T* space known as isomeke, representing all possible entrapment conditions for a given host–inclusion pair. The intersection of isomekes for different inclusions in the same host can provide P-T_{trap}. Omphacite has the advantage of providing, with Raman spectroscopy, not only P_{inc} (Baratelli et al., 2024), but also the closure *T* (Baratelli et al., 2025a) through the cationic order phenomenon. As *T* decreases, omphacite undergoes a cation order process which leads to a splitting of the two sites hosting cations with six and eight coordination number, *M*1 and *M*2 (Fig. 1a), into non-symmetrically related *M*1 and *M*11, and *M*2 and *M*21, respectively (Fig. 1b). As a result, the presence of cationic order lowers the space group symmetry from *C*2/*c* to *P*2/*n*. Thus, the determination of the state of chemically ordered omphacite can constrain the closure *T* and cooling rate experienced by the host rock.

The aim of this study has been to develop the necessary tools to exploit the chemical, structural and elastic properties of omphacite to enable it to be used in elastic geothermobarometry by means of Raman spectroscopy. To achieve this goal, omphacite crystals with different degrees of cationic-site order and different chemical composition were characterised via a multi-methodological approach.

MATERIALS AND METHODS

The omphacite crystals analysed in this study are from Münchberg Mass, Bavaria (O'Brien, 1993), with compositions $Jd_{43}Di_{57}$ and $Jd_{52}Di_{48}$ (where Jd = jadeite, Di = diopside). They belong to the same omphacite samples that have been previously analysed with Infrared spectroscopy and single-crystal X-ray diffraction (SC-XRD) by Boffa Ballaran et al. (1998a, b) and by high-pressure (*HP*) SC-XRD by Pandolfo et al. (2012a, b). All of the crystals were initially analysed with SC-XRD. Fe^{3+}-rich omphacites from

Lugros and Camarate (SE Spain), and Voltri massif eclogites (Italy) (Cámara, 1995; Cámara et al., 1998), along with synthetic Fe-free omphacites (Pandolfo et al., 2015) and a Di and a Jd crystal from the Museum der Natur Hamburg - Mineralogie, were also used for the chemical calibration of omphacites using Raman spectroscopy. These samples were also chemically characterised with Electron Microprobe analysis (EMPA).

Ab initio HF/DFT (Hartree Fock/Density Functional Theory) simulations have been conducted with the CRYSTAL17 software (Dovesi et al., 2018) on a fully ordered $Jd_{50}Di_{50}$ omphacite to explore the structural and the Raman spectra evolution as a function of *P*.

Experiments at non-ambient conditions

In situ H*P* Raman spectroscopic measurements were performed using a diamond anvil cell (DAC). Two sets of experiments were performed, using omphacite crystals with two different compositions ($Jd_{43}Di_{57}$ and $Jd_{52}Di_{48}$) and various states of cation order, obtained through annealing experiments. Single crystals with a low Fe content were selected to avoid further chemical effects on the Raman spectrum. The details of the crystals used in these experiments and presented in the figures are listed in Table 1.

In addition, a H*P* SC-XRD study of a $Jd_{43}Di_{57}$ crystal, up to 10 GPa, was performed at the Xpress beamline of the Elettra Synchrotron, Trieste. The crystal was cut with a focused ion beam in two different perpendicular directions. Both slices were loaded into a DAC to maximize the available reciprocal space information. This allowed us to obtain accurate structural variations in terms of deformation of bonds and coordination polyhedra, necessary to compare these results with the H*P* Raman spectroscopy ones.

Table 1 Details of the crystals used in HP Raman spectroscopy experiments. The symbols listed here are used in the following figures. Q_{M1} and Q_{M2} are the order parameters determined from single-crystal refinements (Q = 1 for ordered and Q = 0 for disordered omphacite). T is the annealing temperature applied for time t in hours.

	Symbol	Q_{M1}	Q_{M2}	Ann. T (°C)	Ann. t (h.)
$Jd_{43}Di_{57}$	■	0.828	0.397		
	■	0.864	0.453		
	□	-	-	900	168
	□	-	-	900	168
$Jd_{52}Di_{48}$	▲	0.863	0.453		
	▲	0.751	0.419	950	1
	▲	0.624	0.318	950	5*
	▲	0.512	0.257	950	2.5
	▲	0.109	0.034	950	45
	△	-	-	950	458

* Shows a lower degree of order, corresponding approximately to an annealing time of 2 h.

RESULTS

Raman spectroscopy

According to the group theory, Raman spectra of disordered omphacites consist of 30 Raman active modes, while ordered omphacites have twice as many modes (Fig. 2). The assignment of each Raman peak to a specific atomic vibration was achieved by HF/DFT simulations. The omphacite spectrum is characterised by three regions: *i)* the bond stretching between Si-O between 1000 and 1030 cm^{-1}; *ii)* the Si–O–Si bond bending given by the most intense peak at about 681 cm^{-1}; *iii)* the lower frequency modes, between 50 and 600 cm^{-1}, related to the lattice vibrations.

The main result of this study is the calibration of the Raman peaks of omphacite as a function of 1) the chemical composition, 2) pressure, and 3) cation order degree, each of which is discussed below.

1. The chemical composition affects the wavenumber of some peaks, which increases with the increase of the Al content (Fig. 3a), allowing omphacites richer in Jd or Di component to be distinguished.
2. The wavenumbers of all Raman active modes increase with the applied *P*. The peak at 681 cm^{-1} shows a linear dependence on P (Fig. 3b); its position is not affected by the cation order but is influenced by the chemical composition.
3. The cation order causes a broadening of the Raman peaks, and it is not influenced by *P*. This is particularly visible in the Full Width at Half Maximum (FWHM) of the peak at 681 cm^{-1}, whose value increases with the increase of disorder in the *M* polyhedra (Fig. 3c).

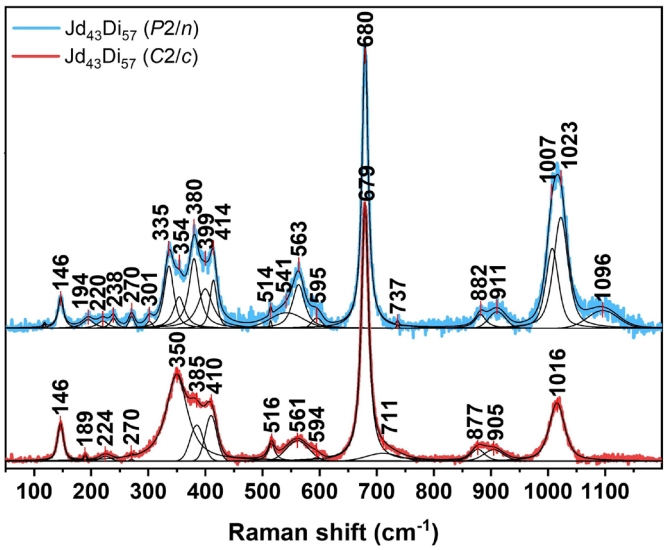

Figure 2 Measured Raman spectra of chemically ordered (light blue line) and disordered (red line) omphacite.

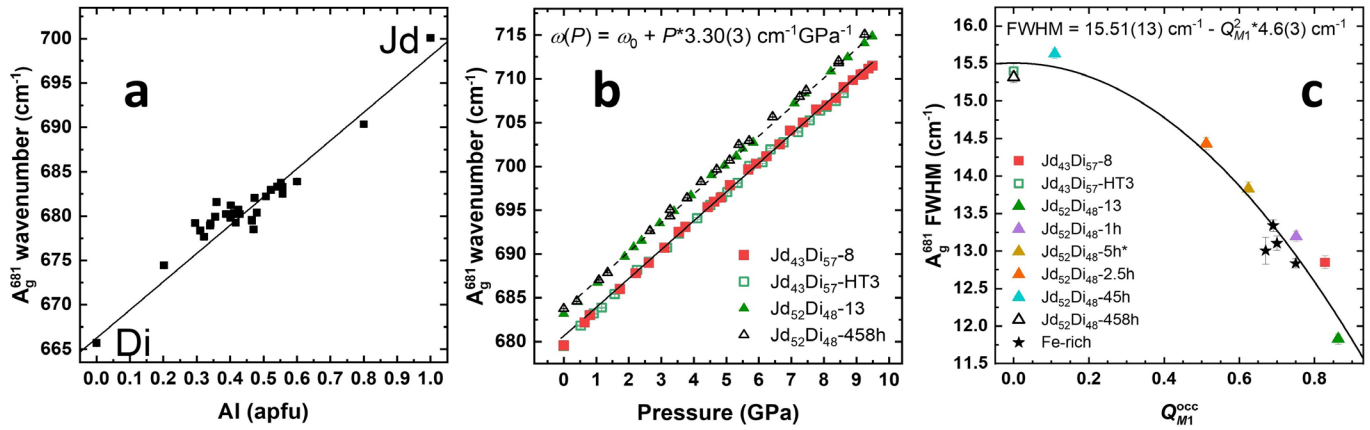

Figure 3 ***a)*** *Chemical composition and* ***b)*** *pressure dependence of the wavenumber of the peak at 681 cm^{-1}. The wavenumber increases linearly with P, but is also influenced by omphacite composition.* ***c)*** *The cation order affects the FWHM of the peak at 681 cm^{-1}, with a parabolic dependence.* ***b)*** *and* ***c)*** *are modified after Baratelli et al. (2025a). Filled symbols are related to ordered omphacites, while open symbols to disordered ones.*

The *P*-dependent behaviour of some Raman peaks exhibited a discontinuity near 5 GPa (*e.g.*, Fig. 4), suggesting a variation in the compression mechanisms occurring in the six- and eight-coordinated sites of the ordered omphacite structure.

HP SC-XRD

To explain the anomalous behaviour of the Raman peaks, H*P* SC-XRD analysis was conducted on an ordered omphacite (with composition $Jd_{43}Di_{57}$) using synchrotron radiation (Baratelli et al., 2025b). The experimental results were compared with *ab initio* simulations. A second-order Birch-Murnaghan (BM) equation of state (EoS) fit of all data yields V_0 = 422.85(15) Å^3, and K_{T0} = 121.3(11) GPa, using the EosFit7 software (Gonzalez-Platas et al., 2016). For the $Jd_{50}Di_{50}$ omphacite, calculated with hybrid HF/DFT simulations, a third-order BM EoS was employed, and the fit of all data yields V_0 = 426.52(3) Å^3, K_0 = 119(2) GPa, and K' = 4.9(5) (Fig. 5a). The results indicate a stabilisation of the *T*2 TILT angle (Fig. 5b), defined as the out-of-plane tilting of the basal face of the tetrahedron with respect to the plane (100) (Cameron et al., 1973), which correlates with distortion variation in the *M*1 octahedron around 3 GPa (Fig. 5c). This coincides with a decrease in the rate of *M*1 deformation under increasing *P*. *Ab initio* simulations indicate that the 337 cm^{-1} mode is related to tetrahedral rotation around the *c* axis, that can be related to the *T*2 TILT angle variation. Thus, both long-range (SC-XRD) and short-range (Raman spectroscopy) analysis supports the observed changes in polyhedral distortion of the *M*1 octahedra. In disordered omphacites, this behaviour cannot be observed due to symmetry constraints: in *C*2/*c* omphacite, only a single *M*1 polyhedron is present, exhibiting an average chemistry between the *M*1 and *M*11 sites of *P*2/*n* structure, resulting in a Raman spectrum that displays fewer Raman active modes.

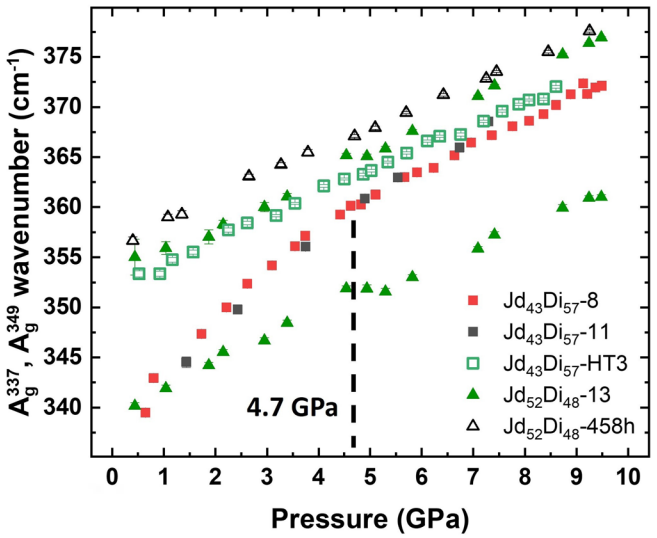

Figure 4 *Pressure dependence of the Raman peaks in the range 335-375 cm^{-1}. For sample $Jd_{43}Di_{57}$ only one peak at 337 cm^{-1} was detected experimentally, with an anomalous behaviour near 4.7 GPa in the ordered crystals. For sample $Jd_{52}Di_{48}$ two peaks were resolved, but an anomaly is still visible. Filled symbols are related to ordered omphacites, while open symbols to disordered ones.*

DISCUSSION

This study represents the first step towards using omphacite inclusions for elastic geothermobarometry via Raman spectroscopy. By knowing the EoS and the composition of the inclusion (determined by EMPA), it is possible to a first approximation to estimate its residual *P* using Raman spectroscopy. To achieve this result, it is essential to study the effects of the chemical composition, *P*, and the cation order. At the current stage, empirical calculations for selected phonon modes can be used for this purpose (see Fig. 3). Once the residual *P* of an omphacite inclusion has been measured, it is necessary to determine the entrapment isomeke. This calculation requires the EoSs of both the host and the inclusion, and the chemical composition plays a crucial role, as it influences the elastic behaviour. In the case of omphacite, for example, Pandolfo et al. (2012a) discussed the compositional dependence of the bulk modulus.

Omphacite-in-garnet is a common host-inclusion system in several geological settings. Due to the greater stiffness of garnet with respect to omphacite, the inclusion undergoes more volume relaxation, generating a

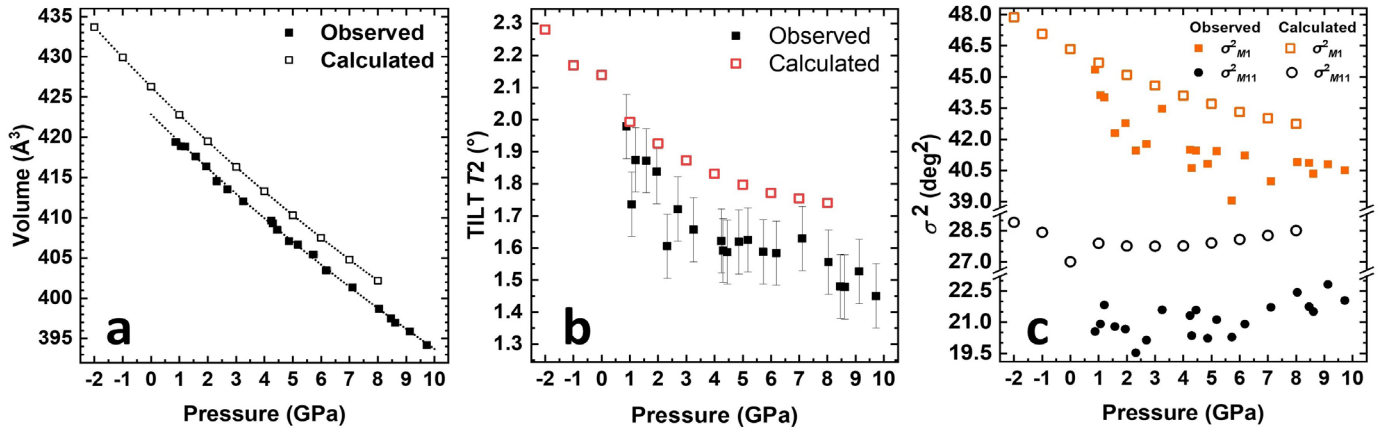

Figure 5 ***a)*** *Pressure evolution of the unit-cell volume of the analysed crystal ($Jd_{43}Di_{57}$) compared with that calculated using HF/DFT methods ($Jd_{50}Di_{50}$).* ***b)*** *Pressure dependence of the TILT angle related to T2; the angle ceases to decrease around 3 GPa.* ***c)*** *Variation of the bond angle variance (σ^2; Robinson et al., 1971) with pressure. The variation is antithetical for the M1 and M11 polyhedra: σ^2_{M1} decreases with pressure, while σ^2_{M11} remains almost constant and starts increasing gradually above 6 GPa. (Baratelli et al., 2025b).*

measurable residual P from which entrapment conditions can be calculated. The isomekes of omphacite resemble those of quartz, making it a potential barometer (Fig. 6). The slope of the isomekes and the phase transition characteristics of the omphacite-in-garnet system offer advantages over quartz- and zircon-in-garnet, expanding the *P-T* range of applicability.

CONCLUSIONS

Omphacite-in-garnet host-inclusion systems could offer important insights in low-*P* and high-*T* geological settings where both quartz and zircon inclusions (among the most used mineral phases in elastic geothermobarometry) in garnet have considerable limitations (Murri et al, 2019; Campomenosi et al., 2022). Omphacite inclusions are particularly valuable in low-silica systems such as metabasites (the main lithotype of eclogites), where quartz is not stable and omphacite becomes a suitable phase for retrieving metamorphic peak conditions.

The use of omphacite inclusions offers a double advantage: they can provide both residual *P* information, through the Raman peak position, and the closure *T*, through the cation ordering phenomenon, which affects the FWHM. The intense Raman peak near 681 cm^{-1} is particularly well-suited for this purpose, as it exhibits a strong *P* dependence, which is not affected by the cation order. Furthermore, HF/DFT calculations indicate that this mode has the highest Raman intensity, ensuring that it can be experimentally detected in any random orientation. Since garnets do not show Raman scattering in this spectral range, this peak is the best candidate to be used for elastic geothermobarometry using omphacite inclusions.

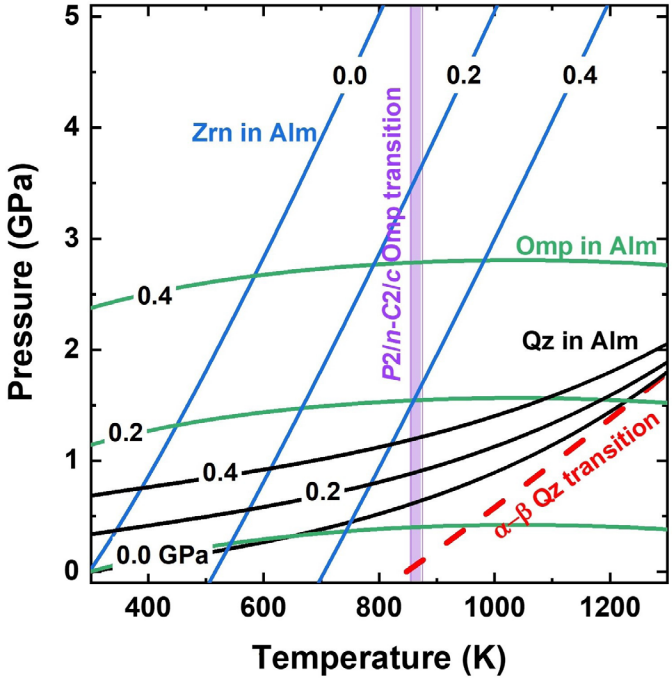

Figure 6 Calculated isomekes for quartz (Qz), zircon (Zrn) and omphacite (Omp) inclusion in an almandine (Alm) host. The α-β quartz and the P2/n-C2/c omphacite transitions are also represented. Modified after Baratelli et al. (2024).

REFERENCES

Angel, R.J., Murri, M., Mihailova, B., Alvaro, M. (2019) - Stress, strain and Raman shifts. Z. Krist.-Cryst. Mater., 234, 129-140.

Baratelli, L., Murri, M., Alvaro, M., Prencipe, M., Mihailova, B., Cámara, F. (2024) - Raman scattering of omphacite at high pressure: towards its possible application to elastic geothermobarometry. Am. Mineral., 109, 2105-2115.

Baratelli, L., Murri, M., Alvaro, M., Mihailova, B., Boffa Ballaran, T., Domeneghetti, M.C., Cámara, F. (2025a) - The effect of cation ordering in omphacite on the phonon compressibility: A step towards Raman elastic geothermobarometry. Chem. Geol., 678, 122650.

Baratelli, L., Merlini, M., Nestola, F., Nava, J., Joseph, B., Prencipe, M., Cámara, F. (2025b) - Determination of local geometrical distortions in an ordered omphacite under high pressure. Mineral. Mag., accepted.

Boffa Ballaran, T., Carpenter, M.A., Domeneghetti, M.C., Tazzoli, V. (1998a) – Structural mechanisms of solid solution and cation ordering in augite-jadeite py-

roxenes: I. A macroscopic perspective. Am. Mineral., 83, 419–433.

Boffa Ballaran, T., Carpenter, M.A., Domeneghetti, M.C., Salje, E.K.H., Tazzoli, V. (1998b) - Structural mechanisms of solid solution and cation ordering in augite-jadeite pyroxenes: II. A microscopic perspective. Am. Mineral., 83, 434–443.

Cámara, F. (1995) - Estudio cristalquímico de minerales metamórficos en rocas básicas del complejo Nevado-Filábride (Cordilleras Béticas). PhD thesis, Universidad de Granada, Granada.

Cámara, F., Nieto, F., Oberti, R. (1998) - Effects of Fe^{2+} and Fe^{3+} contents on cation ordering in omphacite. Eur. J. Mineral., 10, 889–906.

Cameron, M., Sueno, S., Prewitt, C.T., Papike, J.J. (1973) - High temperature crystal chemistry of acmite, diopside, hedenbergite, jadeite, spodumene, and ureyite. Am. Mineral., 58, 594–618.

Campomenosi, N., Angel, R.J., Alvaro, M., Mihailova, B. (2022) - Resetting of zircon inclusions in garnet: Implications for elastic thermobarometry. Geology, 51, 23-27.

Dovesi, R., Erba, A., Orlando, R., Zicovich-Wilson, C.M., Civalleri, B., Maschio, L., R'erat, M., Casassa, S., Baima, J., Salustro, S., Kirtman, B. (2018) - Quantum-mechanical condensed matter simulations with CRYSTAL. Wires. Comput. Mol. Sci., 8(4), e1360.

Gilio, M., Angel, R.J., Alvaro, M. (2021) - Elastic geobarometry: how to work with residual inclusion strains and pressures. Am. Mineral., 106, 1530-1533.

Gonzalez-Platas, J., Alvaro, M., Nestola, F., Angel, R.J. (2016) - EosFit7-GUI: a new graphical user interface for equation of state calculations, analyses and teaching. J. Appl. Crystallogr., 49, 1377–1382.

Momma, K. & Izumi, F. (2008) - *VESTA*: a three-dimensional visualization system for electronic and structural analysis. J. Appl. Crystallogr., 41(3), 653-658.

Murri, M., Alvaro, M., Angel, R.J., Prencipe, M., Mihailova, B.D. (2019) - The effects of non-hydrostatic stress on the structure and properties of alpha-quartz. Phys. Chem. Miner., 46, 487-499.

O'Brien, P.J. (1993) - Partially retrograded eclogites of the Munchberg Massif, Germany: records of a multi-stage Variscan uplift history in the Bohemian Massif. J. Metamorph. Geol., 11, 241-260.

Pandolfo, F., Nestola, F., Cámara, F., Domeneghetti, M.C. (2012a) - New thermoelastic parameters of natural C2/c omphacite. Phys. Chem. Miner., 39, 295–304.

Pandolfo, F., Nestola, F., Cámara, F., Domeneghetti, M.C. (2012b) - High-pressure behavior of space group P2/n omphacite. Am. Mineral., 97, 407–414.

Pandolfo, F., Cámara, F., Domeneghetti, M.C., Alvaro, M., Nestola, F., Karato, S.I., Amulele, G. (2015) - Volume thermal expansion along the jadeite–diopside join. Phys. Chem. Miner., 42, 1–14

Robinson, K., Gibbs, G.V., Ribbe, P.H. (1971) - Quadratic Elongation: A Quantitative Measure of Distortion in Coordination Polyhedra. Science, 172, 567-570.